SUPERCONDUCTING α-FeSe STUDIED BY MÖSSBAUER SPECTROSCOPY AND MAGNETIC MEASUREMENTS

A. Błachowski[1], K. Ruebenbauer[1*], J. Żukrowski[2], J. Przewoźnik[2], K. Wojciechowski[3], and Z. M. Stadnik[4]

[1]Mössbauer Spectroscopy Division, Institute of Physics, Pedagogical University
PL-30-084 Cracow, ul. Podchorążych 2, Poland
[2]Solid State Physics Department, Faculty of Physics and Applied Computer Science,
AGH University of Science and Technology
PL-30-059 Cracow, Al. Mickiewicza 30, Poland
[3]Department of Inorganic Chemistry, Faculty of Material Science and Ceramics,
AGH University of Science and Technology
PL-30-059 Cracow, Al. Mickiewicza 30, Poland
[4]Department of Physics, University of Ottawa, Ottawa, Ontario K1N 6N5, Canada

[*]Corresponding author: sfrueben@cyf-kr.edu.pl

Problems of modern techniques in engineering and education - 2009; eds. P.Kurtyka, P.Malczewski, K.Mroczka, and K.Ziewiec; Institute of Technology, Pedagogical University, Cracow 2009; p. 15-20

Abstract: Superconducting FeSe has been investigated by measurements of the magnetic susceptibility versus temperature and Mössbauer spectroscopy at various temperatures including strong external magnetic fields applied to the absorber. It was found that dominant defects for the sample having excess iron are iron atoms intercalated between iron selenium sheets. A transition from the *P4/nmm* to the *Cmma* structure lowers electron density on the intercalated iron atom by $0.86\,\text{electron}\,\text{a.u.}^{-3}$. Hence, two-dimensional character of the structure is enhanced in the *Cmma* structure in comparison with the higher temperature *P4/nmm* structure. Mössbauer measurements in the external magnetic field and for temperatures below transition to the superconducting state revealed null electron spin density within the unit cell. Hence, the compound behaves like Pauli paramagnet taking into account susceptibility data and Mössbauer results. The principal component of the electric field gradient on the iron nucleus was found as negative on the regular iron sites.

Keywords: iron-based superconductor, Mössbauer spectroscopy, paramagnetism

1. Introduction

Recent discovery of the iron-based superconductivity [1] resulted in the great scientific activity in similarity to the previous discovery of the high temperature superconductivity in cuprates [2]. Iron-based superconductors belong to pnictides or chalcogenides and these compounds have been already investigated in the past [3-5]. The simplest superconductor of this class belongs to the iron-selenium system, as it is simple binary system [6]. There are several compounds in the iron-selenium system [7], but superconductivity has been discovered for a compound being formed close to the FeSe stoichiometry. The following crystal phases could form close to the above composition range: 1 the tetragonal *P4/nmm* structure, 2 the hexagonal $P6_3/mmc$ structure similar to the NiAs with various defects, and 3 the hexagonal phase (Fe_7Se_8 formal composition) with two distinctly different kinds of defect order, i.e., *3c* or *4c* [8]. Phase 2 is hard to obtain, as it is basically disordered phase 3. The kind of order in the phase 3 depends on the cooling rate from the high temperature [8]. All of

the above phases order magnetically except tetragonal phase 1. Magnetic transition temperatures lie above room temperature except for the NiAs type phase 2. The latter orders above liquid nitrogen temperature and the magnetic ordering process is accompanied by the lowering of the crystal symmetry [9]. A tetragonal phase transforms into *Cmma* orthorhombic phase between 100-80 K [10-11]. A tetragonal phase could be prepared with excess iron. It is formed within narrow temperature range and it transforms to the phase 2 upon heating above 450 °C [3]. Superconductivity has been discovered for this metallic phase with excess iron and the transition temperature lies within the stability range of the orthorhombic phase. It seems to depend on the stoichiometry [12]. It depends strongly on the applied pressure and dopants [13, 14]. An orthorhombic phase transforms to the hexagonal phase for very high pressures [14]. Efforts to prepare samples containing pure tetragonal phase 1 failed. It is always contaminated by some amount of either phase 3 or 2 and by some amount of the metallic α-Fe. Usually traces of Fe_3O_4 occur as well.

There are several questions to be addressed for the tetragonal/orthorhombic $Fe_{1+x}Se$ system. The first point is concerned with the location of the excess iron. It is unlikely to have iron on the regular selenium sites in this layered structure. Hence, one can expect either some structural vacancies on the selenium lattice and completely filled iron lattice or some interstitial iron in addition to perfect iron and selenium lattices. The model with intercalated interstitial iron as dominant defects is favored, but no real proof of its applicability exists. Due to the random distribution of defects this question has to be addressed by some shortsighted method. Another important question is concerned with the electron spin density on iron. The Mössbauer spectroscopy seems particularly useful here, as iron makes the basic constituent of the compound. The same method is able to address both problems provided susceptibility is measured in the low field and Mössbauer spectra are obtained in the strong external magnetic field – preferably below transition to the superconducting state.

We report here on the preparation of the tetragonal phase, X-ray powder diffraction, susceptibility measurements and investigation by using Mössbauer spectroscopy.

2. Experimental

The sample was prepared by applying direct reaction between iron and selenium. Iron powder (AlfaAesar 99.5 % purity, 99.9+ % metal base) having spherical particles below 10 μm diameter was reduced under flow of 15 % of H_2 and 85 % of Ar mixture for one hour at 500 °C in the silica tube. A formal stoichiometry was chosen as $Fe_{1.053}Se$. Hence, proper amount of selenium (AlfaAesar 99.999+ % purity) in the form of shots having 2-4 mm size and reduced iron was sealed in the evacuated silica tube in order to prepare sample of 2 g. The tube was enclosed in another evacuated silica tube. A synthesis was carried at 750 °C for six days. Subsequently the sample was slowly cooled with the furnace to the room temperature. Resulting ingot was powdered in the mortar, powder sealed in the evacuated silica tube, and the sample was annealed at 420 °C for 48 hours and subsequently quenched in the ice water.

Powder X-ray diffraction pattern was obtained at room temperature by using Siemens D5000 diffractometer. The Cu-Kα radiation was used with the pyrolytic graphite monochromator on the detector side. Data were analyzed by means of the Rietveld method as implemented in the FULLPROF program [15].

Magnetic susceptibility was measured by means of the vibrating sample magnetometer (VSM) of the Quantum Design PPMS-9 system. The pelletized sample having mass 66.046 mg was cooled in the zero external magnetic field (no more than 0.7 Oe) to 2 K. It was subsequently warmed up to 355 K in the applied field of 5 Oe. Susceptibility was measured in the sweep mode in the field of 5 Oe during cooling sample having above history down to 2 K. Afterwards susceptibility was measured versus increasing temperature to 305 K in the field of 5 Oe.

Mössbauer spectra were collected at room temperature (RT), 80 K, 4.2 K and in the external magnetic field oriented along the γ-ray beam axis. Spectrum for the field 5 T was recorded with the source and absorber at 5.0(8) K, while the spectrum for the field 9 T was recorded with the source and absorber at 4.7(1) K. For the remaining measurements ^{57}Co(Rh) source was kept at room temperature. All shifts are reported versus room temperature metallic iron. Data were analyzed by means of the MOSGRAF program [16].

3. Results

Figure 1 shows diffraction pattern. A tetragonal α-FeSe phase *P4/nmm* makes 93.7(6) % contribution. It has the following lattice constants *a*=3.7720(1) Å and *c*=5.5248(1) Å. The hexagonal phase makes 4.3(2) % contribution. It has been fitted as *P6₃/mmc* disordered structure with the following lattice constants *a*=3.643(1) Å and *c*=5.909(2) Å. However Mössbauer data indicate that in fact it is one of the Fe_7Se_8 structures. Some traces of the magnetite (*a*=8.397(1) Å) and metallic iron (*a*=2.867(1) Å) were found as well.

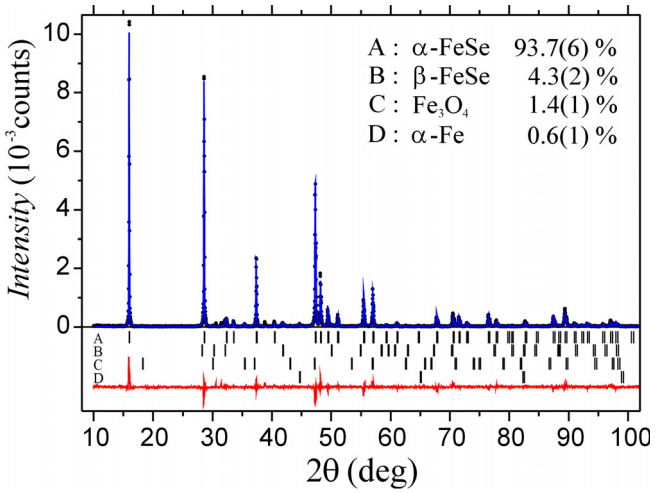

Fig. 1. Powder X-ray diffraction pattern obtained at room temperature and by using Cu-Kα radiation. The pattern was obtained for the scattering angle 2θ varying between 10-158 deg.

Mössbauer spectra obtained at room temperature (RT) and 80 K for high velocity ranges are shown in Figure 2 together with magnetic field distributions obtained for the magnetically ordered components by means of the Hesse-Rübartsch method [17].

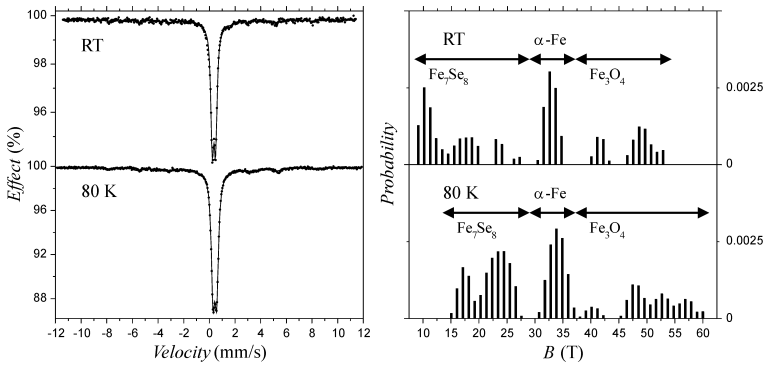

Fig. 2. Mössbauer spectra obtained for high velocity ranges together with the iron hyperfine field distributions in the minor phases. Non-magnetic contribution due to the dominant phase (tetragonal at RT and orthorhombic at 80 K) is fitted as single doublet on this velocity scales.

The spectrum is dominated by the non-magnetic component originating in the tetragonal (RT) or orthorhombic phase (80 K) undergoing to the superconducting state at low temperatures. Field distribution clearly shows contribution from magnetite and one can even see Vervey transition upon cooling sample to 80 K. A contribution originating in the metallic iron is clearly seen as well. Additionally there are many small fields evolving to higher fields upon cooling with marked change in the distribution shape. They correspond to the fields expected for the Fe_7Se_8 structure including spin rotation upon cooling [18]. Hence, we conclude that the hexagonal phase is of the Fe_7Se_8 type (probably *3c* according to the thermal history of the sample). Therefore all minor phases are already magnetically ordered at room temperature with hyperfine fields not smaller than 10 T.

Results of the magnetic susceptibility measurements are shown in Figure 3. One can see spin rotation in the hexagonal phase at about 125 K [18]. Vervey transition in magnetite does not

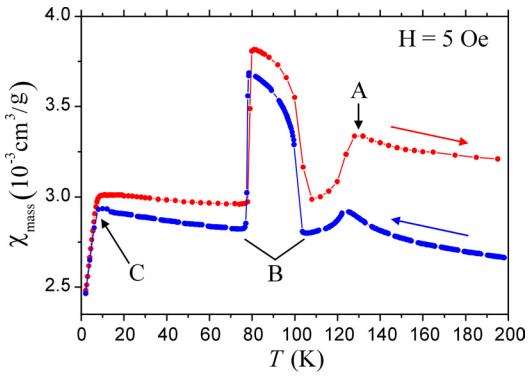

show up. A transition from the tetragonal *P4/nmm* structure to the orthorhombic *Cmma* structure starts at about 100 K, and it is completed before reaching temperature 80 K. Finally, one can see transition to the superconducting state in the *Cmma* phase at about 8 K. The susceptibility very weakly depends on the temperature in the *Cmma* phase above transition to the superconducting state. This is indication of the electron gas paramagnetism in this metallic phase, i.e., for the Pauli paramagnetism.

Fig. 3. Magnetic susceptibility measured upon cooling and subsequent warming of the sample in the field of 5 Oe. The point A corresponds to the spin rotation in the hexagonal phase, region B shows transformation between tetragonal and orthorhombic structures, while point C shows transition to the superconducting state.

Figure 4 shows Mössbauer spectra obtained at RT, 80 K and 4.2 K for low velocity ranges. These spectra were evaluated within transmission integral approximation. The RT spectrum has to be fitted with two doublets in order to obtain reasonable fit quality. No singlet belonging to the *P6$_3$/mmc* could be found [5] and therefore one can be confident that this phase is practically absent. Essential fit results are summarized in Table 1. Dominant doublet is due to the iron in the *P4/nmm* regular tetrahedral sites. One has to realize that in the *P4/nmm* and *Cmma* structures there is single crystallographic regular iron site per unit cell [11], i.e., all regular iron sites are equivalent within the chemical unit cell. Hence, we conclude that the second doublet is due to the excess iron intercalated between iron selenium layers in the octahedral sites. Due to the fact that the wave-vector transfer is rather small for the resonant line used one cannot expect large differences in the recoilless fractions between sites. Hence, the relative intensities of two doublets reflect respective occupancies. Upon cooling to 80 K one obtains *Cmma* structure without any changes in occupancies, of course. Dominant doublet experiences practically some second order Doppler shift (SOD) without significant change of the hyperfine interactions. Minor doublet exhibits change in the isomer shift of the order $+0.249$ mm/s (upon correction for SOD) leading to lowering of the electron density on the iron nucleus by 0.86 electron a.u.$^{-3}$ [19]. Such change would be impossible for the regular iron associated with the selenium vacancy, as the iron selenium layer is distorted in the very minor way during this transition. Hence, one can be confident that the minor doublet is due to the intercalated iron. One has to note that transition to the *Cmma* structure lowers electron density on the intercalated iron, i.e., lowers electron density in the region between layers enhancing two-dimensional character of the electron structure. No changes occur upon further cooling to 4.2 K except variation in SOD contribution.

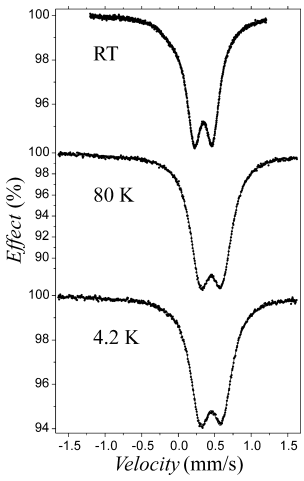

Fig. 4. Mössbauer spectra obtained for low velocity ranges.

Figure 5 shows spectra obtained in the external magnetic fields of 5.0 T and 9.0 T and below superconducting transition temperature. Spectra were fitted averaging over direction between the magnetic field and principal axis of the electric field gradient (EFG) in one deg steps due to the powder form of the absorber [16]. External field is much higher than the first critical field and practically all iron nuclei experience applied field. Data evaluation reveals that hyperfine fields on both iron sites are exactly equal to the applied

field, i.e., 4.99(1) T and 8.96(1) T, respectively. Hence, there is no magnetic moment on the iron nuclei. Due to the fact that intercalated iron is distributed over various sites one can conclude that the electron spin density equals null within the whole unit cell. We have assumed that EFG is axially symmetric.

Table 1. Essential results obtained by using Mössbauer spectroscopy. The spectra were processed within the transmission integral approximation. The symbol *A* stands for the relative contributions of two doublets obtained from the RT spectrum and kept constant in the remaining fits. The symbol *S* denotes total spectral shift of the respective component versus RT metallic iron. The symbol Δ stands for the quadrupole splitting, while the symbol Γ denotes absorber linewidth common for all lines.

T (K)	*A* (%)	*S* (mm/s)	Δ (mm/s)	Γ (mm/s)
RT	91(1) 9(1)	0.457(1) 0.225(2)	0.261(1) 0.418(3)	0.147(1)
80 K	91 9	0.564(1) 0.581(4)	0.274(1) 0.46(1)	0.202(2)
4.2 K	91 9	0.562(1) 0.586(6)	0.283(1) 0.44(1)	0.212(2)

This assumption is valid for the regular iron sites surrounded by selenium, and probably acceptable for the intercalated iron. We have found negative value for the principal component of the EFG on the regular iron sites. It is hard to determine sign for the intercalated iron as it contributes relatively weakly to the spectrum. Somewhat better fit is obtained for the positive value.

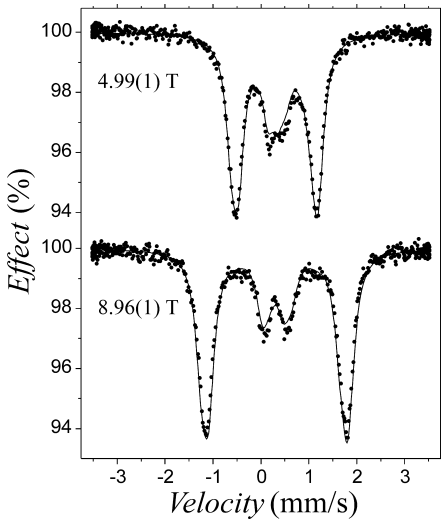

Fig. 5. Mössbauer spectra obtained in the external magnetic field aligned with the beam. Spectrum for the field 5.0 T was recorded with the source and absorber at 5.0(8) K, while the spectrum for the field 9.0 T was recorded with the source and absorber at 4.7(1) K. Field values shown in Figure are obtained from the fit of spectra.

4. Conclusions

There are two basic conclusions obtained upon having performed above investigations:

1. Dominant defects for excess iron are formed as intercalated iron on the octahedral sites between iron selenium layers. The electron density between iron selenium layers lowers upon transition to the orthorhombic phase making system more two-dimensional.
2. There is no net electron spin density in the unit cell.

Therefore it seems unlikely that spin or orbital momentum contributions are responsible for pairing electrons into Cooper pairs. It seems as well that one has standard Cooper pairs with null spin (S=0) as otherwise some magnetic moment would be likely to be seen on the iron nucleus. Similar results were obtained by the Mössbauer measurements in the external magnetic field for $LaFeAsO_{0.89}F_{0.11}$ [20], $La_{0.87}Ca_{0.13}FePO$ [21], $LaFeAsO_{0.93}F_{0.07}$ [21] and other iron-based superconductors like filled skutterudites ($LaFe_4P_{12}$) [22]. Mössbauer measurements on the metallic-like $Fe_{1.04}Se$ sample in the 5 T field at 4.2 K did not show any appreciable contribution due to the internal hyperfine magnetic field on iron [3]. Similar results were obtained for non-stoichiometric insulator $Fe_{1+x}S$ [23] and many other low-spin

ferrous and insulating compounds like cyanides. The situation is somewhat different for the superconducting high-pressure hexagonal ε-Fe [24], where the external field being able to destroy superconductivity induces a hyperfine field on the iron nucleus far beyond the limit of the Knight shift [25]. The Knight shift for the iron-based superconductors investigated up to now by ^{57}Fe (14.41-keV line) Mössbauer spectroscopy is below detection limit by this method.

References

1. Y. Kamihara, T. Watanabe, M. Hirano, and H. Hosono, J. Am. Chem. Soc. **130**, 3296 (2008).
2. J. G. Bednorz and K. A. Müller, Z. Phys. B **64**, 189 (1986).
3. T. Tsuji, A. T. Howe, and N. N. Greenwood, J. Solid State Chem. **17**, 157 (1976).
4. B. K. Jain, A. K. Singh, and K. Chandra, J. Phys. F: Metal Phys. **8**, 2625 (1978).
5. K. V. Reddy and S. C. Chetty, Phys. Stat. Sol. (a) **32**, 585 (1975).
6. F-C. Hsu, J-Y. Luo, K-W. Yeh, T-K. Chen, T-W. Huang, P. M. Wu, Y-C. Lee, Y-L. Huang, Y-Y. Chu, D-C. Yan, and M-K. Wu, Proceedings of the National Academy of Sciences **105**, 14262 (2008).
7. T. B. Massalski, *Binary Alloy Phase Diagrams*, vol. 1, 2nd ed., ASM International, Materials Park, Ohio, USA, 1990, p. 1769.
8. H-N. Ok, K-S. Baek, and E-C. Kim, Solid State Commun. **87**, 1169 (1993).
9. W. Schuster, H. Mikler, and K. L. Komarek, Monatshefte für Chemie, **110**, 1153 (1979).
10. S. Margadonna, Y. Takabayashi, M. T. McDonald, K. Kasperkiewicz, Y. Mizuguchi, Y. Takano, A. N. Fitch, E. Suard, and K. Prassides, Chem. Commun. **43**, 5607 (2008).
11. T. M. McQueen, A. J. Williams, P. W. Stephens, J. Tao, Y. Zhu, V. Ksenofontov, F. Casper, C. Felser, and R. J. Cava, arXiv:0905.1065 (2009).
12. T. M. McQueen, Q. Huang, V. Ksenofontov, C. Felser, Q. Xu, H. Zandbergen, Y. S. Hor, J. Allred, A. J. Williams, D. Qu, J. Checkelsky, N. P. Ong, R. J. Cava, Phys. Rev. B **79**, 014522 (2009).
13. Y. Mizuguchi, F. Tomioka, S. Tsuda, T. Yamaguchi, and Y. Takano, Appl. Phys. Lett. **93**, 152505 (2008).
14. S. Medvedev, T. M. McQueen, I. Trojan, T. Palasyuk, M. I. Eremets, R. J. Cava, S. Naghavi, F. Casper, V. Ksenofontov, G. Wortmann, and C. Felser, arXiv:0903.2143 (2009).
15. J. Rodriguez-Carvajal, Physica B **192**, 55 (1993).
16. K. Ruebenbauer and T. Birchall, Hyperfine Interact. **7**, 125 (1979); see also: www.elektron.ap.krakow.pl
17. J. Hesse and A. Rübartsch, J. Phys. E: Sci. Instrum. **7**, 526 (1974).
18. J. S. Yang, D. H. An, K. U. Kang, D. H. Kim, K. S. Baek, and H. N. Oak, J. Korean Phys. Soc. **35**, 492 (1999).
19. U. D. Wdowik and K. Ruebenbauer, Phys. Rev. B **76**, 155118 (2007).
20. S. Kitao, Y. Kobayashi, S. Higashitaniguchi, M. Saito, Y. Kamihara, M. Hirano, T. Mitsui, H. Hosono, and M. Seto, J. Phys. Soc. Japan **77**, 103706 (2008).
21. S. Higashitaniguchi, M. Seto, S. Kitao, Y. Kobayashi, M. Saito, M. Kurokuzu, T. Mitsui, Y. Yoda, Y. Kamihara, M. Hirano, and H. Hosono, J. Phys. Soc. Japan **78**, 024704 (2009).
22. G. P. Meisner, Physica B+C **108**, 763 (1981).
23. D. J. Vaughan and M. S. Ridout, J. Inorg. Nucl. Chem. **33**, 741 (1971).
24. K. Shimizu, T. Kimura, S. Furomoto, K. Takeda, K. Kontani, Y. Onuki, and K. Amaya, Nature **412**, 316 (2001).
25. R. D. Taylor, G. Cort, and J. O. Willis, J. Appl. Phys. **53**, 8199 (1982).